# Observations of a comet tail disruption induced by the passage of a CME

T. A. Kuchar,[1] A. Buffington,[2] C. N. Arge,[3] P. P. Hick,[2] T. A. Howard,[4,5] B. V. Jackson,[2] J. C. Johnston,[3] D. R. Mizuno,[1] S. J. Tappin,[6] and D. F. Webb[1]

[1] The Solar Mass Ejection Imager observed an extremely faint interplanetary coronal mass ejection (ICME) as it passed Comet C/2001 Q4 (NEAT) on 5 May 2004, apparently causing a disruption of its plasma tail. This is the first time that an ICME has been directly observed interacting with a comet. SMEI's nearly all-sky coverage and image cadence afforded unprecedented coverage of this rarely observed event. The onset first appeared as a "kink" moving antisunward that eventually developed knots within the disturbed tail. These knots appeared to be swept up in the solar wind flow. We present the SMEI observations as well as identify a likely SOHO/LASCO progenitor of the CME. SMEI observed two other comets (C/2002 T7 [LINEAR] and C/2004 F4 [Bradfield]) and at least five similar events during a 35-d period encompassing this observation. Although these had similar morphologies to the 5 May NEAT event, SMEI did not observe any ICMEs in these cases. Three of these were observed close to the heliospheric current sheet indicating that a magnetic boundary crossing may have contributed to the disruptions. However, there are no discernable causes in the SMEI observations for the remaining two events.

## 1. Introduction

[2] Comet plasma tails have been used as in situ probes of the heliosphere ever since they were used as evidence for the existence of the solar wind [*Biermann*, 1951]. A plasma tail is confined by the solar wind magnetic field, which is draped around the comet [*Brandt and Chapman*, 2004, and references therein]. Therefore the tail's appearance is directly influenced by the flow and direction of the solar wind.

[3] During the spring of 2004 the Solar Mass Ejection Imager (SMEI) [*Eyles et al.*, 2003; *Jackson et al.*, 2004] observed three comets simultaneously: C/2004 F4 (Bradfield), C/2001 Q4 (NEAT), and C/2002 T7 (LINEAR). The latter two underwent at least six major plasma tail disruptions within a 35-d period. The tail of Comet Bradfield, however, remained quiescent throughout the period.

[4] SMEI's primary mission is to detect and track solar disturbances in the heliosphere, including corotating structures and ICMEs. It provides nearly continuous monitoring of the entire sky with a sensitivity ($\sim$0.2 $S_{10}$, $S_{10}$ = the brightness of a 10th magnitude solar-type star per square degree) sufficient to detect very faint ICMEs. As a space-based imager, SMEI is in a unique position to make many serendipitous observations of other transient phenomena and had an unprecedented view of these tail disruptions. Similar observations have been primarily ground-based and thus were constrained by observing conditions (e.g., sky background and rising/setting times). Unhampered by such constraints SMEI was able to observe these events for many hours (up to 2 d) and over great distances (in some cases over several tens of degrees).

[5] One particular event on 5 May 2004 involving Comet NEAT occurred simultaneously with the passage of an ICME. We present a detailed analysis of this event and identify a likely candidate for the CME progenitor at the Sun. These observations along with preliminary results were first reported by *Kuchar et al.* [2006]. In section 2 we present a brief description of the SMEI instrument and the image processing procedures. Section 3 discusses an overview of all the comet observations but the section primarily focuses on the 5 May disruption and the CME associated with it. Section 4 discusses the implications for

[1]Institute for Scientific Research, Boston College, Chestnut Hill, Massachusetts, USA.

[2]Center for Astrophysics and Space Sciences, University of California, San Diego, La Jolla, California, USA.

[3]Air Force Research Laboratory, Space Vehicles Directorate, Hanscom AFB, Massachusetts, USA.

[4]Physics Department, Montana State University, Bozeman, Montana, USA.

[5]Now at Space Vehicles Directorate, Air Force Research Laboratory, Sunspot, New Mexico, USA.

[6]National Solar Observatory/Sacramento Peak, Sunspot, New Mexico, USA.

the HCS crossing paradigm and section 5 summarizes our conclusions.

## 2. SMEI Instrument and Data Processing

[6] The SMEI mission and data processing [*Jackson et al.*, 2004] as well as the instrument design and testing [*Eyles et al.*, 2003] are discussed elsewhere; therefore, only a brief summary will be provided here. *Tappin et al.* [2004] reported on the first Earth-directed CME observed by SMEI and discussed the analysis for tracking interplanetary disturbances. A catalog of CMEs observed during the first 18 months of SMEI operations is presented in the work of *Webb et al.* [2006].

[7] SMEI is part of the US Air Force Space Test Program's Coriolis mission, which was launched on 6 January 2003. The Coriolis satellite was placed into a Sun-synchronous polar orbit with an altitude of 840 km and a period of 102 min. The SMEI instrument consists of three baffled CCD cameras, each with a $60° \times 3°$ field of view. The fields overlap giving a nearly $160°$ long strip that sweeps out nearly $4\pi$ steradians per orbit. CCD frames are recorded at 4-s intervals. At this cadence, a patch of sky is typically image about 10 times. Ground processing corrects the data for observational and systematic effects [*Jackson et al.*, 2004] before registering the data on a standard celestial grid with a resolution of $0.1°$. Approximately 14 all-sky maps are produced per day. SMEI brightness is typically given in telemetered counts of analog-to-digital units (ADU). A surface brightness of one S10 corresponds to $0.46 \pm 0.02$ ADUs over one square degree in a SMEI sky map [*Buffington et al.*, 2007].

[8] At times, the comet tails extended some tens of degrees and were seen at extreme ecliptic latitudes. To reduce projection distortions at the ecliptic poles the SMEI data were imaged as "fisheye" projections. We chose a standard FITS (Flexible Image Transport System) [*Calabretta and Greisen*, 2000] representation (zenithal equidistant) which maintains a constant angular scale along the radius of the image. These images (cf. Figure 1) are Sun-centered with a radius of $135°$ about the Sun, which covers the extent of observations before the comets or their disrupted tails faded from view. The image pixels are $0.5°$ bins with a resolution of $\sim1°$. At this level of processing each image bin is the average of approximately 10 CCD frames providing an RMS sensitivity of $\sim0.1$ ADU [*Buffington et al.*, 2006].

[9] SMEI's sunward camera (Camera 3) has a solar zone of avoidance with a radius of approximately $20°$. Hence, all the sky maps have a corresponding circular gap near the Sun. Since the axis of SMEI's orbit is fixed in declination, the Sun moves within this circle and occasionally into the field of view of the Camera 3 for different portions of the orbit during the year. This camera is shuttered during these latter periods to protect the CCD but the CCD becomes saturated before the shutter is closed.

[10] The celestial and zodiacal background is brighter by several orders of magnitude than the phenomena SMEI was intended to detect and is removed for this study using a baseline of, at most, 12 orbits (six previous and six subsequent). At each sky position four of the five minimum pixels in the baseline were averaged after disregarding the lowest. The backgrounds were calculated and removed

using the high-resolution $(0.1°)$ celestial grid images and then reprojected as the fisheye images.

[11] Figure 1 shows a typical fisheye image with a Sun-centered ecliptic grid superimposed. Note the substantial portion displayed beyond $90°$ elongation, including the $45°$ areas around the ecliptic poles. Along with NEAT, the two other comets (Bradfield and LINEAR) are also visible. The position of the Moon, which tends to saturate several CCD frames when in or near the field of view of the camera, is also indicated. Approximately 35 d of images from 24 April to 28 May were processed in this manner. A time-lapse movie for this time period, showing the progression of these comets, is provided as supporting online material (Movie S1)[1].

## 3. Comet and CME Observations

[12] The SMEI images primarily show the plasma tails of all three comets. Their dust tails appeared, at most, $1°-2°$ in length and were almost indistinguishable from the comae at the SMEI resolution. Both Comets NEAT and LINEAR displayed an almost continual billowing in their plasma tails during the analyzed period. Comet Bradfield's tail, however, appeared quiescent throughout its observation. The tails of NEAT and LINEAR exhibited the typical "disturbed" appearance for comets in the highly variable solar wind flow around the Sun's equatorial region (in heliographic coordinates rather than the ecliptic coordinates displayed in Figure 1). SMEI observed Bradfield only at high heliographic latitudes ($>60°$ north), which placed it in the fast and steady solar wind flow typical of the Sun's polar region during this declining phase of the solar cycle. This accounts for its essentially featureless tail in the SMEI observations. *Brandt and Snow* [2000] have cataloged many comets displaying the same characteristics in these two zones of solar wind flow.

[13] Along with the billowing of their tails, SMEI observed several "tail disruptions" for both NEAT and LINEAR. The disruptions appear as an abrupt change in the orientation of the plasma tail which propagates anti-sunward and away from the comets undisturbed tail. Table 1 lists six of the major events, all of which have similar morphologies. The date, time (UT), solar elongation, and position angles of the onset of the disruption are measured from the SMEI images. The geocentric ecliptic and heliographic coordinates (in degrees) were obtained from the respective comets' ephemerides. All of these events were observed while the comets were on the Earth-facing side of the Sun. The last two columns of Table 1 list the distances of the comets to the Sun and the Earth (in astronomical units, also from the ephemerides) at the time of the disruptions.

### 3.1. NEAT Disruption Event of 5 May 2004

[14] Comet NEAT was at a heliocentric distance of $\sim1$ AU during the analysis period. Closest approach to the Earth occurred on 6 May, when it came within 0.32 AU. The comet was a naked eye object during a portion of the SMEI observations and was easily visible in the SMEI images without the background processing described in section 2.
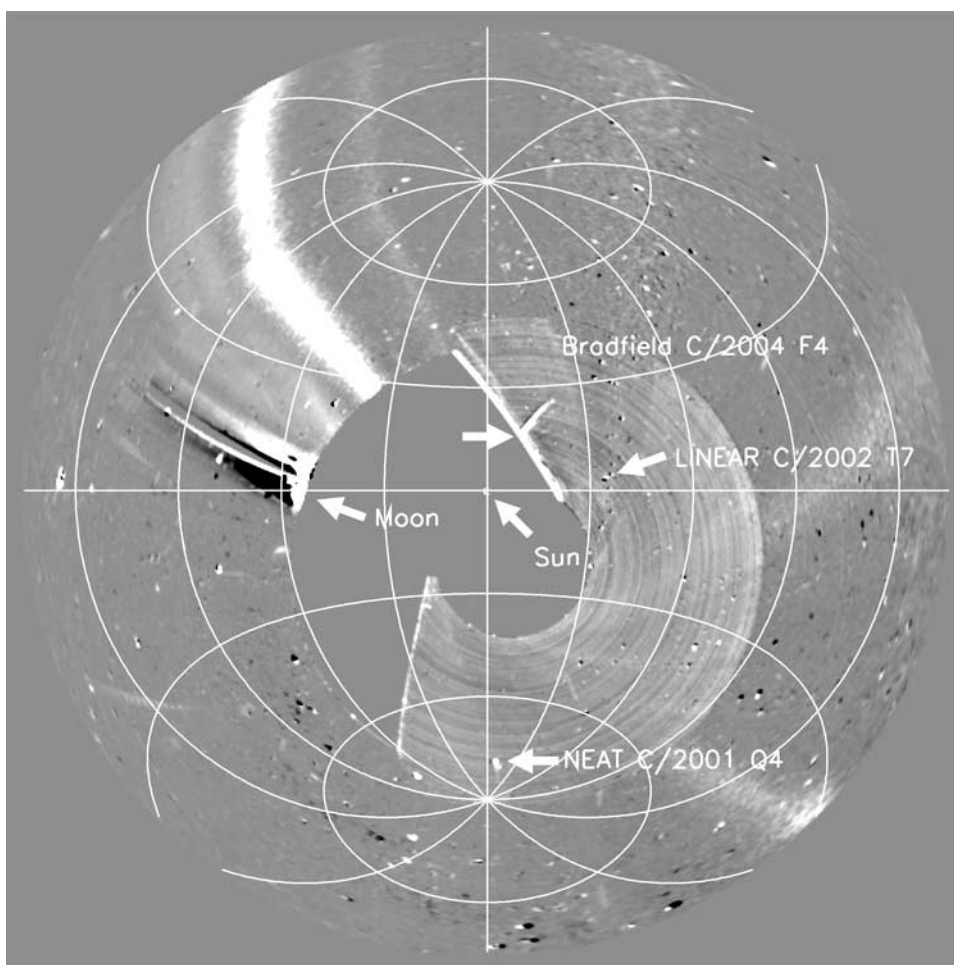
**Figure 1.** The positions of the three comets as observed by SMEI are shown in a background-subtracted "fisheye" image. The image is cast in ecliptic coordinates and displays out to a radius of 135° from the Sun. The coordinate grid is spaced every 30° in both longitude and latitude. The range in the grayscale is ±8 ADU. The Sun's position is indicated as is the area of saturation caused by the Moon. The 20° solar exclusion zone is below and slightly right of center. The large wedge of missing (shutter-closed) data to the left of center is due to the Sun's proximity to Camera 3, the sunward facing camera. The transient white bands that occasionally appear in the images result from particle and light contamination from the auroral ovals [*Mizuno et al.*, 2005]. This is the first frame of a time-lapse movie provided as supporting online material (Movie S1).

However the full extent of its plasma tail became evident after the background was removed, revealing a tail that reached nearly 35° on 4 May. By comparison, a web search of ground-based observations showed NEAT with a tail ~7° in length, which would cover 14 image bins in Figure 1. Although this faint, extended component of the plasma might be obscured by the sky in ground-based observations, SMEI had sufficient sensitivity to observe it throughout the analysis period and during the disruptions.

[15] With some exceptions, ground-based observations of comet plasma tails extend to only several degrees. It is apparent from the SMEI observations that the fainter extremes of the tails can reach much farther. However, arc-minute-sized structures seen in ground-based observa-

**Table 1.** SMEI Disruption Observations of 2004

| | | | | | | Geocentric Ecliptic Coords. | | Heliographic Coords. | | Distances (AU) | |
|---|---|---|---|---|---|---|---|---|---|---|---|
| Event | Date | DOY | Time | Elong. | Pos. Ang. | Long. | Lat. | Long. | Lat. | Sun-Comet | Earth-Comet |
| NEAT 1 | 26 Apr | 117 | 0130 | 84.9 | 177.1 | 50.687 | −80.035 | 78.314 | −35.914 | 1.02 | 0.47 |
| NEAT 2 | 5 May[a] | 126 | 0030 | 80.3 | 140.8 | 117.752 | −50.224 | 305.754 | −19.179 | 0.98 | 0.33 |
| LINEAR 1 | 13 May | 134 | 1830 | 57.6 | 237.8 | 358.619 | −25.865 | 234.163 | −10.411 | 0.76 | 0.35 |
| LINEAR 2 | 14 May | 135 | 1450 | 55.8 | 230.8 | 4.964 | −31.149 | 218.379 | −11.317 | 0.77 | 0.33 |
| LINEAR 3 | 18 May | 139 | 1700 | 51.0 | 185.3 | 49.573 | −52.140 | 148.678 | −15.499 | 0.82 | 0.27 |
| LINEAR 4 | 26 May | 147 | 1100 | 77.0 | 129.7 | 137.810 | −38.690 | 19.875 | −17.887 | 0.93 | 0.40 |

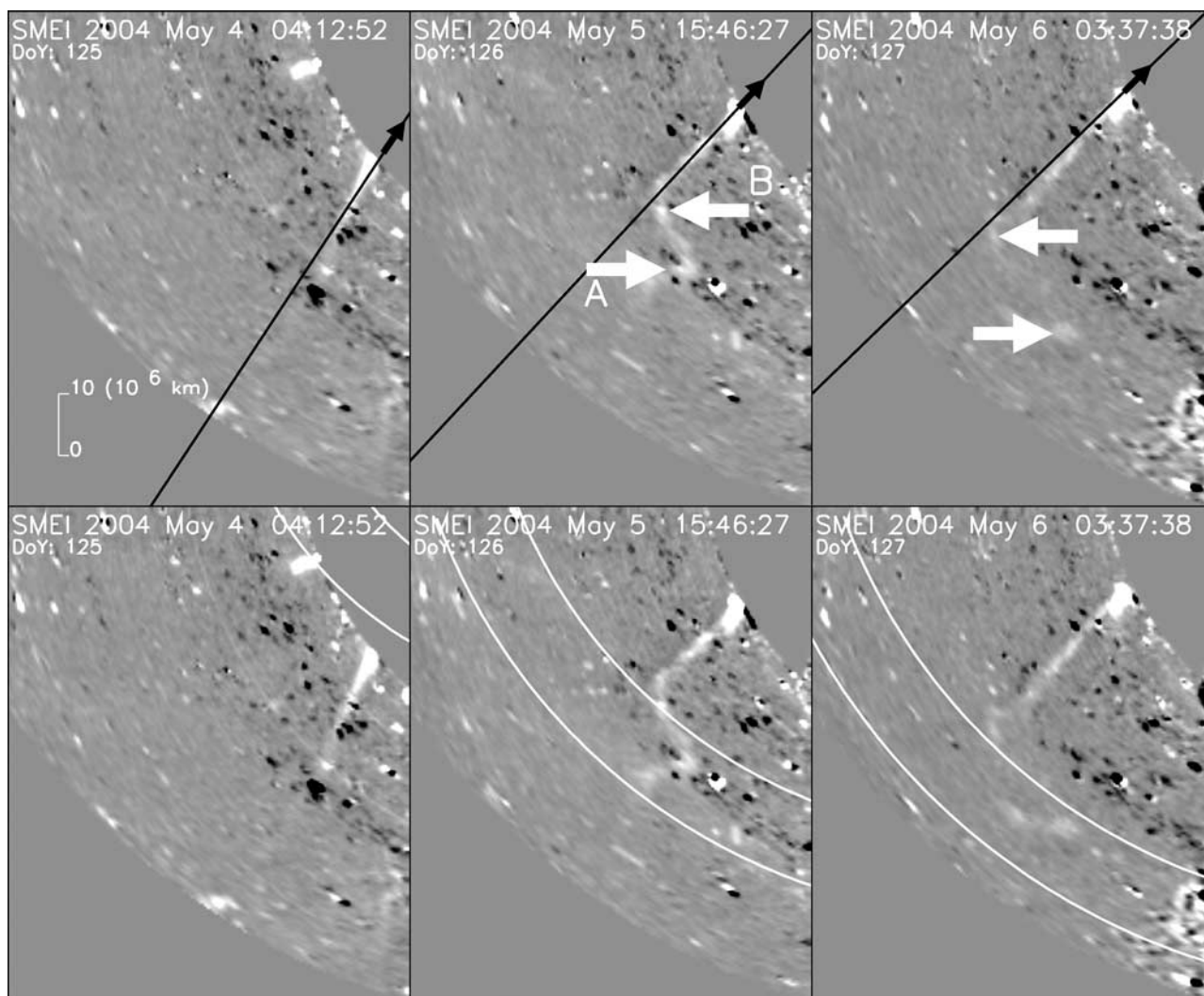[a]Observation examined in detail in the text.

**Figure 2.** The top panels show sections of three fisheye images before and during the comet tail disruption. The onset is estimated to have occurred at 0030 UT on 5 May. The white arrows indicate the locations of the tail fragments tracked for elongation-time measurements (see Figure 3). The black line indicates the radial direction to the Sun and is drawn through the position of the comet as determined by the comet ephemeris. The linear scale provided in the top left panel is based on the comet's distance from the Earth (0.32 AU) at the time of the event and is corrected for foreshortening. This scale is only applicable along the Sun-comet line due to the projection geometry. The bottom three panels show the same images with the position of the observed ICME marked by the two arcs. The projected path of the ICME is derived from mean values of the elongation/time measurements of the ICME presented in Figure 4 and summarized in Table 2. The distance between the two arcs is 15°, which is the maximum measured width for the ICME. All the images are scaled at ±3 ADU to highlight the fainter portions of the comet tail and the knots with in it. These three panels are frames of a time-lapse movie, which is scaled for the ICME and provided as online supporting material (Movie S2).

tions would be unresolved and blended with other tail features in the SMEI imaging. Therefore, it may prove difficult to find exact analogs in the SMEI observations to structures seen at much higher angular resolution in the ground-based images. For instance, it is possible that some of the SMEI tail disruptions may be the downtail progression of disconnection events, blurred by SMEI's limited angular resolution. Moreover, we do not necessarily preclude that in some cases, SMEI may also be observing other types of heliospheric/plasma tail interactions.

[16] Figure 2 shows sections from a sequence of three fisheye images detailing the 5 May comet NEAT disruption. The onset was first observed at 0030 UT and appeared simply as a "kink" in the tail. However, the onset may have begun earlier, as a portion of the comet was in the closed shutter region covered by Camera 3. As it progressed, the kink grew more pronounced while it propagated downwind of the tail. Although somewhat exaggerated by the distortion of the fisheye projection, the apparent stretching of this kink, almost perpendicular to the line marking the comet's unperturbed tail, is a real effect. Portions of the kink
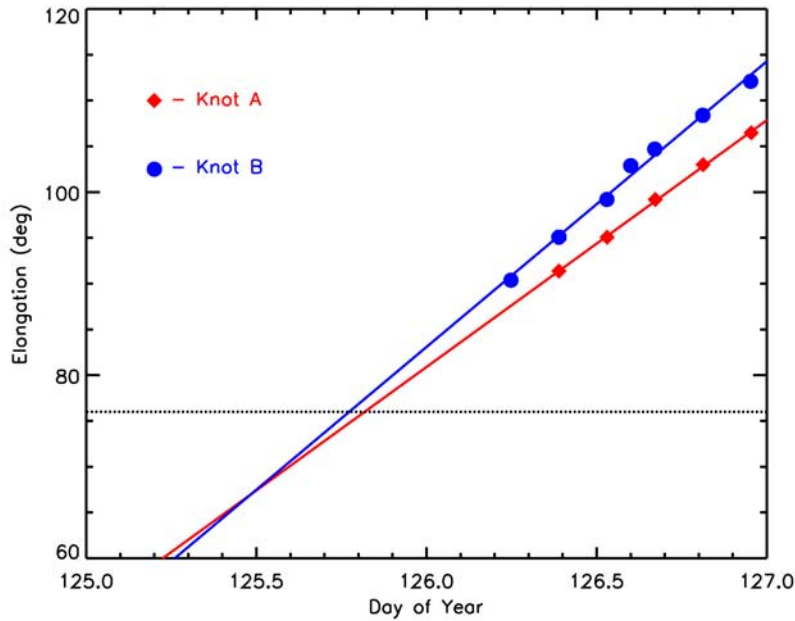
**Figure 3.** The solar elongations of the two tail knots, as indicated by the arrows in Figure 2, are plotted with time. The solid lines represent linear fits to these data. The dashed horizontal line represents the solar elongation of the comet nucleus, which remained approximately constant during the disruption. A summary of the results from the fits are presented in Table 2.

developed knots (i.e., isolated, compact regions within the fainter tail as denoted by the white arrows in Figure 2), some of which momentarily brightened as if being compressed. These knots continued to move down wind but also away from the comet as it moved in its orbit, suggesting that they may have been swept up by the solar wind flow. The plasma tail upwind of the kink also developed knots but otherwise remained relatively intact. A time-lapse movie detailing this event is provided as supporting online material (Movie S2).

[17] Some of these knots could still be seen trailing away up to 48 h after the onset of the event. The scale of this disruption was quite extensive, stretching over 60° of the sky and thus over several tens of millions of kilometers. A linear scale, based on the comet's distance at the onset of the disruption, is provided at the left in Figure 2 and is corrected for foreshortening. Since the images have a pronounced azimuthal distortion as a result of the sky projection (fish-eye) geometry, the scale is only applicable along the Sun-comet line (the dark arrow and line in Figure 2).

[18] Two of the brighter knots (denoted by A and B in Figure 2) in the kink were tracked for several SMEI orbits following their development. Their solar elongations are plotted with respect to time in Figure 3. The dashed line in Figure 3 indicates the solar elongation of the comet nucleus, which was relatively constant during the disruption. A linear fit was performed to estimate their angular speeds: 28° and 31°/d, respectively. For an Earth-comet distance of 0.33 AU, these translate to linear speeds of 300 and 330 km/s after correcting for foreshortening. It should be noted that this is only the velocity component along the knot/Sun line. There is likely to be an additional component in the direction of the observer imparted by the driving force of the disruption (determination of which is beyond the scope of this paper).

However, any azimuthal velocity component must be small in comparison as the knots drifted very little ($\sim$2°) during the observation of the disruption.

[19] SMEI also observed a faint ICME passing the comet just prior to the disruption. This ICME is cataloged as the 2004 DOY (day of year) 125 event in Table 1 of *Webb et al.* [2006]. The ICME was just visible above SMEI's $3\sigma$ noise limit and appeared as a broad, featureless arc spanning about 60°. Since Figure 2 was scaled specifically to show the comet tail, the ICME is difficult to discern even when the images are appropriately scaled for it. However, its motion makes it more perceptible to the eye when single images are looped in a time-lapse fashion (see Movie S2).

[20] We attempted to identify the CME progenitor for this ICME using the Large-Angle Spectroscopic Coronagraph (LASCO) [*Brueckner et al.*, 1995] image archive and the CME catalog [*Yashiro et al.*, 2004] at http://cdaw.gsfc. nasa.gov/CME_list/index.html. This period was fairly active and the archive contained several possible CMEs. We developed a list of CME candidates that fell within a search window provided by not only the position and timing of the ICME but that of the comet tail disruption as well.

[21] The launch time of the CME was estimated from elongation-time measurements of the ICME in the SMEI data. Since the ICME lacked any distinguishable features to track, measurements were made at several position angles along its approximate leading edge. These data are plotted in Figure 4 for three locations along the arc with their respective linear fits. Table 2 summarizes the fits for ICME measurements along with the two tail knots. The table lists the position angles of the measurements, the angular speeds, and the projected CME launch time at the Sun (0° elongation). Uncertainty in the angular speeds is $\sim\pm2$°/d which is mostly due to variations in the measurements. The data in
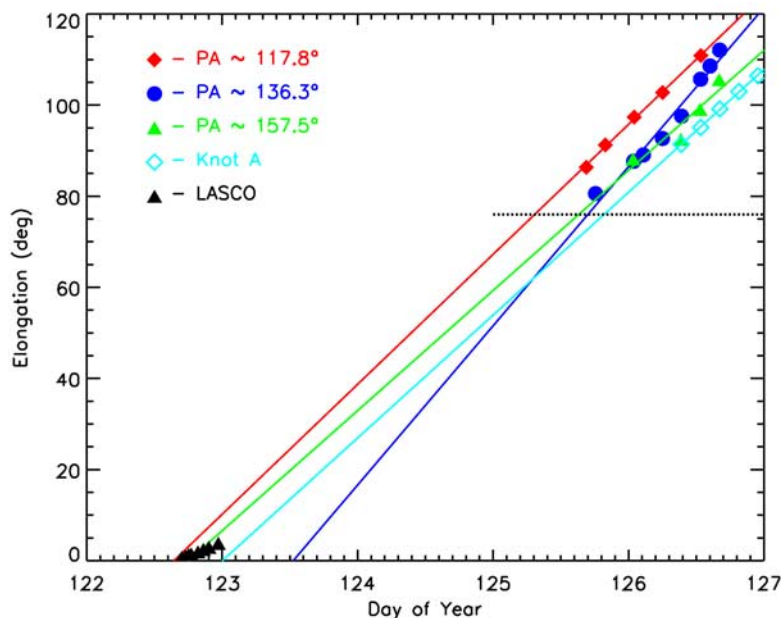
**Figure 4.** The solar elongations are plotted with time as measured for three positions along the leading edge of the SMEI-observed ICME. The lines represent linear fits to these data. A summary of the fits is presented in Table 2. The measurements from the associated LASCO CME near the sun are also shown. For comparison the measurements of the comet tail Knot A and the elongation of the comet nucleus (dashed line) are also plotted.

Table 2 provide an approximate launch time; however, a CME may accelerate or decelerate when it enters the solar wind flow. Therefore candidates were chosen using a reasonable time interval around 1–2 May (DOY 122–123). Approximate launch locations on the Sun for the candidate CMEs were determined by associating each with a surface feature. Since the disturbance was required to propagate in the direction of the ICME and toward the comet, the comet's position in heliographic coordinates placed restrictions on the geometry and origin on the Sun for the candidate CMEs.

[22] Table 3 lists the best candidate that satisfied these criteria for the second NEAT event: a partial halo, associated with an X-ray flare, observed on 1 May 2004 at 1650 UT. The table lists parameters for the CME as observed by LASCO and includes the day and time the CME was first seen in C2, the position angle of the CME with respect to the solar disc (measured counterclockwise from north), the angular span of the CME, its derived plane of sky speed, surface association, and the heliographic coordinates of the surface feature. The height-time measurements for this CME are included in Figure 4. The nearly 70° gap in the figure is due to the proximity of the Sun to Camera 3, causing the camera to be shuttered during this event.

[23] One of the main uncertainties in making CME/ICME associations is determining the propagation direction of the CME. It is possible that some of the other candidate CMEs could be directed toward the comet and yet not interacting with it. Given this uncertainty in the identification process and the 70° coverage gap, it is difficult to determine which, if any, of the other CMEs are actually directed toward the comet. However, SMEI directly observed only this ICME at the comet.

[24] The development of a kink in the plasma tail may be indicative of a shearing effect where the flow past the comet changes speed and/or direction. As noted above, the solar wind flow is highly variable in this area of the heliosphere but nonradial flows are also possible. *Owens and Cargill* [2004] surveyed nonradial flows in the solar wind and found almost half of the large flows (>100 km/s) were associated with ICMEs. Since it is difficult to see the ICME in relation to the comet in individual images, the parameters in Table 2 (speed ∼30°/d, launch time ∼122.9 DOY) were used to plot a schematic of the ICME on the lower three panels of Figure 2. The long axis of the kink appears to align with (in projection) the ICME. Along with the measurements plotted in Figure 4 this shows that the timing and speed of the kink and embedded knots compare well with the ICME, supporting the visual impression that the passing ICME caused the disruption.

[25] As shown in Movie S2 and emphasized in Figure 2 the leading edge of the ICME passes by the comet just prior to the tail disruption. If the disruption is to be initiated at this boundary, this suggests the arc observed in SMEI may not be at the same location as the comet. *Vourlidas and Howard* [2006] have demonstrated that at large solar elongations the brightest portion of an ICME may not be

**Table 2.** Results of Elongation/Time Linear Fits

|  | Position Angle (deg) | Speed (deg/d) | Launch Time (DOY) |
|---|---|---|---|
| ICME position 1 | 117.8 ± 0.6 | 28.9 | 122.65 |
| ICME position 2 | 136.3 ± 0.2 | 34.9 | 123.52 |
| ICME position 3 | 157.5 ± 1.1 | 26.4 | 122.75 |
| Comet fragment A | 138.9 ± 1.8 | 28.0 | - |
| Comet fragment B | 144.3 ± 0.9 | 31.2 | - |

**Table 3.** LASCO CME Candidates for Disruption Associations

| Comet Event | Date (2004) | Time (UT) | Pos. Ang. (deg) | Span (deg) | Speed (km/s) | Surface Association | CME Direction Heliographic Long. (deg) | Lat. (deg) | Notes |
|---|---|---|---|---|---|---|---|---|---|
| NEAT 2 | 1 May | 1650 | 218 | 138 | 342 | X-ray flare C9.5 class | 330 | −11 | partial halo |
| LINEAR 1 | 10 May | 0426 | 251 | 136 | 413 | X-ray flare B1.9 class | 331 | −19 | partial halo |
| LINEAR 2 | 10 May | 1950 | 232 | 113 | 316 | EIT flare ∼1700 | 315 | −20 | |
| LINEAR 3 | 15 May | 2050 | 133 | 115 | 280 | none | N/A | N/A | measurements assume CME moving in the same direction as the disruption |
| LINEAR 4 | 23 May | 1106 | halo | 360 | 281 | small EIT eruption | 330 | −9 | NRL reports CME is backsided |
| LINEAR 4 | 24 May | 0626 | 132 | 76 | 451 | none | N/A | N/A | measurements assume CME moving in the same direction as the disruption |

its leading edge. The apparent lag in time between the SMEI-observed arc passing NEAT and the onset of tail disruption may be due to this effect. In this case, the actual ICME front may take slightly longer to reach the comet from SMEI's perspective. Although this scenario is likely, three-dimensional reconstruction of the ICME would be required to confirm this. However, such modeling is beyond the scope of this paper.

[26] In situ data from the Magnetic Field Experiment (MAG) [*Smith et al.*, 1998] and the Solar Wind Electron Proton Alpha Monitor (SWEPAM) [*McComas et al.*, 1998] instruments on board the Advanced Composition Explorer (ACE) spacecraft were examined for possible shocks. The data were searched for shocks within a day of the onset of the disruption and 2 d prior; however, none was evident. The solar wind speed was ∼350 km/s at that time and was decreasing slightly. NEAT was 0.98 AU distant from the Sun at the time of the disruption, which is comparable to the distance of ACE at Earth's $L_1$ point (∼0.99 AU). However, NEAT was also significantly distant from $L_1$ (∼0.33 AU) such that a shock at NEAT might not be simultaneously detected at ACE.

[27] The launch speed of the CME (342 km/s, column 6 of Table 3) was derived from the height-time measurements of the LASCO data and therefore is as projected on the skyplane near the Sun. This speed is slower than that needed to reach the comet (∼500 km/s) at the onset of the disruption, which suggest that either the projected speed is too low or that the CME accelerated after entering the solar wind flow.

### 3.2. CME Associations With the Other Disruption Events

[28] The other events listed in Table 1 appeared very similar to the 5 May NEAT disruption. Each began with a kink which propagated down wind and eventually developed knots. The knots also lagged behind the comet and some momentarily brightened. Since this behavior was so similar to the ICME passage in the 5 May event, the SMEI data were searched for additional ICMEs that might be associated with the remaining events. However, the SMEI data at its current level of processing did not reveal any ICMEs within their detection limit.

[29] The LASCO data were similarly searched for CMEs that might be associated with the other events. The positions of the comets and elongation-time measurements of the knots were used in lieu of actual measurements of a SMEI-observed ICME. The use of the knots, however, increases the uncertainty of the launch time from the Sun as the

timing of the disruption appears to lag behind the passage of an ICME based on the 5 May NEAT disruption (see Figures 2 and 4). The best CME candidates for these events are also presented in Table 3. There were no LASCO data available for the first NEAT event. Although the timing and direction of the candidate CMEs match well for the first two LINEAR disruptions, the associations with the latter two are much less certain since no surface associations could be used to determine a launch direction. Identification of a CME for the fourth LINEAR disruption was further complicated because of two possible candidates. However, the CME catalog of alerts compiled by the Naval Research Laboratory [*St. Cyr et al.*, 2000] indicates that the 23 May CME candidate was primarily directed away from the Earth (i.e., backsided).

[30] The ACE data were also examined for shocks for these events. There was insufficient evidence for shocks for the first NEAT and the first and third LINEAR events. Although, slight changes in the magnetic field and solar wind speed were recorded for the second and fourth LINEAR events, evidence of strong shocks was lacking. However, with the possible exception of the third LINEAR event, the comets and the disruption events were sufficiently far from either the Earth-Sun line that the ACE data were probably not relevant.

### 4. Discussion

[31] We interpret the passage of the ICME observed by SMEI as the cause of the disruption of Comet NEAT's plasma tail on 5 May 2004. This is based not only on the spatial and temporal coincidence of the two events but also the development of the kink and its embedded knots; namely the alignment of the long axis of the kink parallel to the trailing edge of the ICME. That we see the knots trailing behind the leading edge of the ICME suggests that the disruption occurred somewhere behind this front. It is possible that the visible front was associated with a shock or its sheath driven ahead of the ICME itself. A disruption of the plasma tail might have been caused by a polarity reversal within the magnetic structure of the ICME, such as a flux rope, trailing the visible portion of the ICME. Alternatively, the disruption of the plasma tail could result from other perturbations (i.e., density changes or velocity shears) either within the ICME or the ambient solar wind.

[32] Recently, *Jones and Brandt* [2004] reported on three cases of tail disturbances of comet 153P/Ikeya-Zhang that they associated with passages of ICMEs observed earlier as fast CMEs in LASCO images. These were interpreted as the
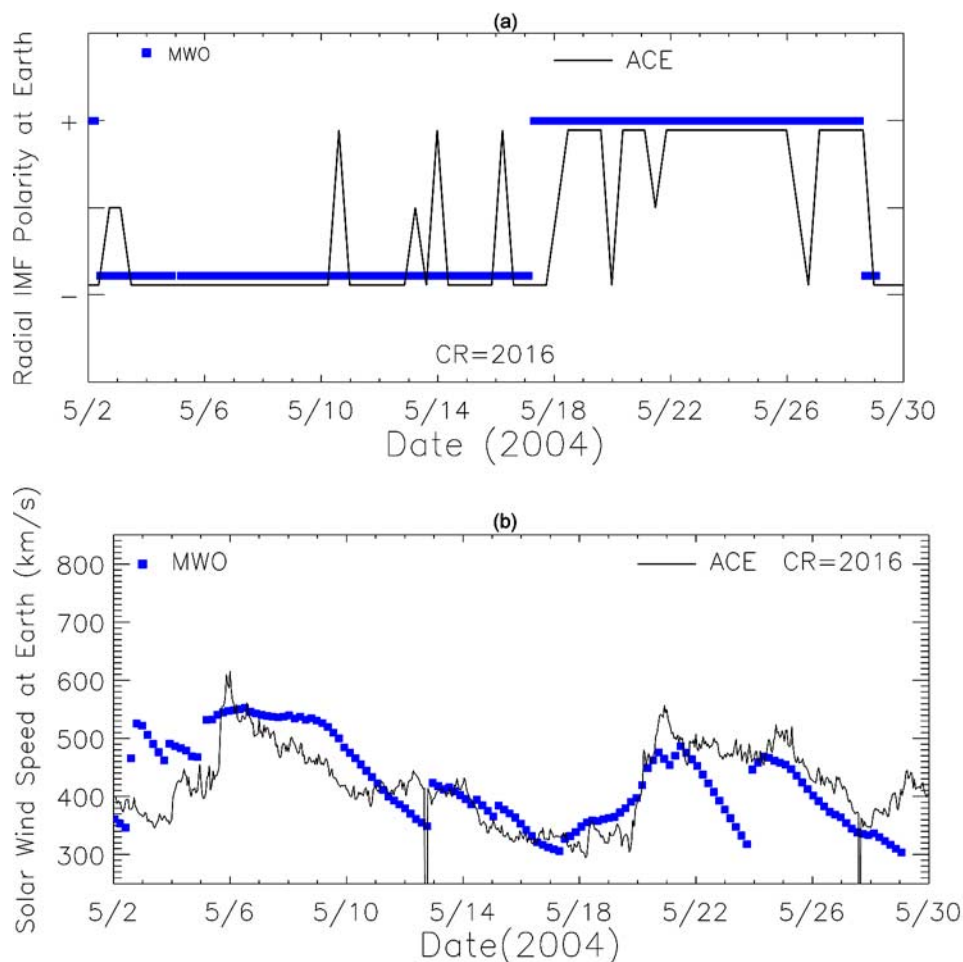
**Figure 5.** (a) The solar wind IMF polarity observations (thin solid back line) from the ACE satellite with Wang-Sheeley-Arge (WSA) model [*Arge et al.*, 2004] predictions (blue line) for Carrington Rotation (CR) 2016. (b) The solar wind speed observations (thin black solid line) from the ACE satellite with WSA predictions (small blue squares) for CR 2016.

draping of ICME magnetic fields around the comet tail. In several cases the images suggested that the draped ICME fields could produce miniature tail condensations and lateral tail shifts. This is similar to what was observed in the SMEI images, although at much larger scales and with less resolution. In contrast, the Jones and Brandt images were collected from various ground-based sources and have arc-minute resolutions typical of ground-based data. These images show the comet's tail ranging from 3° to 8°. At present, there are no other observations attributed to comet-CME interactions although there are some discussions on how those interactions might proceed [*Yi et al.*, 1996; *Wegmann*, 2000]. How an ICME interacts with comet plasma tail will probably depend on the differences in the speeds and the magnetic fields (in direction and strength) of the ICME relative to the ambient solar wind.

[33] Since the orbits of both LINEAR and NEAT covered a wide range of heliographic latitudes, we also considered crossings of the heliospheric current sheet (HCS) as possible triggers for these events. An HCS crossing is presently the paradigm for a disconnection event (DE) as these events can contain the appropriate magnetic field reversals to remove a

magnetically confined plasma tail from its parent comet. *Brandt and Snow* [2000] found that comet DEs tracked well with HCS crossings. *Brandt et al.* [1999] were able to associate all 19 DEs observed in Halley's Comet with HCS crossings. Thus it is important to investigate whether HCS crossings may have influenced the SMEI-observed events.

[34] The position of the HCS was determined using the Wang-Sheeley-Arge (WSA) model [*Arge et al.*, 2004]. WSA is an empirically based model that uses ground-based line-of-sight (LOS) observations of the Sun's surface magnetic field (the Mount Wilson Solar Observatory LOS photospheric magnetic field synoptic map) as input to a magnetostatic potential field source surface (PFSS) model [*Schatten et al.*, 1969; *Altschuler and Newkirk*, 1969]. The PFSS model determines the coronal field out to 2.5 $R_\odot$. The output of the PFSS model serves as input to the Schatten Current Sheet (SCS) model [*Schatten*, 1971], which provides a more realistic magnetic field topology of the upper corona. In this particular study, the magnetic field source surface was extended from 2.5 $R_\odot$ to 5 $R_\odot$, since the field is relatively uniform in field strength by 5 $R_\odot$ and shows little variation beyond the HCS boundary.
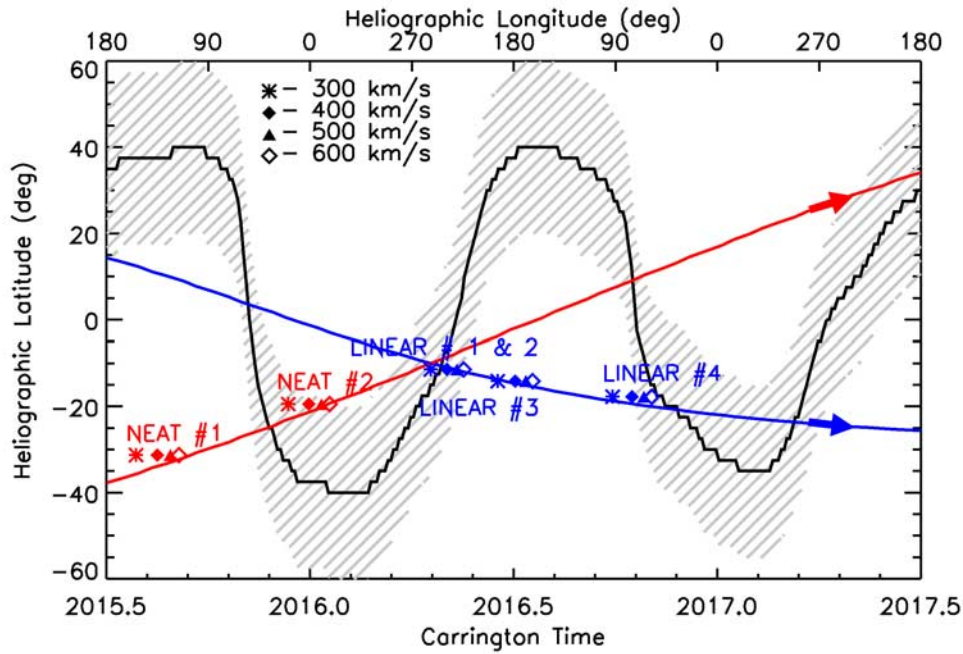
**Figure 6.** The position of the heliospheric current sheet (HCS) at 5 $R_\odot$ is plotted, based on the WSA model. The solid black line indicates where the magnetic field reverses polarity. The hatched area marks a region within 20° of the HCS where disconnection events are likely to occur. The positions of the comets at the time of their tail disruptions are traced back to 5 $R_\odot$ for four possible solar wind speeds. The orbits for NEAT and LINEAR (red and blue lines, respectively) are provided as a guide but are not traced back for any particular solar wind speed. The Carrington longitude (CL) is related to the Carrington time (i.e., a fraction of a solar rotation, CT) and Carrington Rotation number (CR) through the relation: CT = CR + (360° − CL)/360°.

[35] To estimate how well the WSA model reproduces the global structure of the solar wind, we compared the model's predictions of the solar wind speed and interplanetary magnetic field (IMF) polarity with measurements from ACE for Carrington Rotation (CR) 2016. The results from the SCS model were fed into a 1-D modified kinematic code [*Arge and Pizzo*, 2000] which propagates the solar wind out to 1 AU and accounts for stream interactions. In Figure 5a, the ACE IMF polarity observations (black lines) are compared with WSA model predictions (small blue squares). As can be seen, the predicted and observed IMF polarities agree rather well. In Figure 5b, the WSA model solar wind speed predictions are compared with ACE observations. On the whole, the model reproduces the observed solar wind speed reasonably well with only a few discrepancies (e.g., 20−22 May). These results provide us with a relatively high degree of confidence that the model is accurately reproducing (at least in the ecliptic) the structure of the solar wind for this period.

[36] The orbits of the comets were traced back along the solar wind Parker spiral (neglecting stream interactions) to the outer boundary of the coronal portion of the WSA model at 5 $R_\odot$. Since the actual solar wind flow is unknown at the locations of the comets, the positions are traced back assuming four constant speeds from 300 to 600 km/s. Figure 6 shows the locations of the two NEAT and four LINEAR events with respect to the HCS. The first two LINEAR events occurred in rapid succession and the points

mostly overlap at the plotted scale. The modeled HCS boundary at 5 $R_\odot$ is plotted along with the orbits of NEAT and LINEAR. The position of the HCS is determined to within ∼±2.5° in latitude and longitude, which is one grid cell of the WSA model.

[37] On the basis of the *Brandt et al.* [1999] results for the 19 Halley DEs, we determined that the comets need to be within ∼20° of the HCS for an interaction to be likely. Brandt et al. showed that excursions from the HCS by as much as 26° could still result in a DE. However, if the events beyond 20° are excluded, the average distance from the HCS for the Halley DEs is ∼10°. The shaded area in Figure 6 denotes a region within 20° of HCS where interactions with LINEAR and NEAT are likely to occur.

[38] The trace-back for the first NEAT event placed it at least 60° from the HCS, indicating that a boundary crossing did not occur regardless of the true solar wind speed. The trace back of the first two and fourth LINEAR events indicate that a boundary crossing cannot be ruled out as a possible influence, since some of the solar wind speeds place the comet well within 20° of the HCS. However, the trace back for the third LINEAR event placed it too far (at least 50°) from the HCS for any value of the solar wind speed. In the interest of completeness, the second NEAT disruption occurred approximately 20° from the HCS.

[39] The location of the HCS can also be used to indicate the boundaries of other regions that may affect the appearance of the comet tails. The base of the HCS in the low

corona is usually considered to be formed by the streamer belt observed at the Sun [*Smith*, 2001]. The streamer belt is sometimes characterized by large changes in the solar wind flow, which could also result in disruptions in the comet tails. Therefore determining the locations of the comets with respect to the streamer belt is akin to back-projecting them to the Sun at a height of 5 $R_\odot$ and comparing them with the location of the HCS. Although not a precise analog, Figure 6 (with the above analysis) can also indicate which disruptions may be influenced by the streamer belt.

## 5. Conclusions

[40] We have presented coincident observations made by SMEI of an ICME passing Comet NEAT during a plasma tail disruption on 5 May 2004. We associate this passage as the trigger of this event. SMEI observed at least five other disruptions which appeared similar to the NEAT event but without any SMEI-observed ICMEs. From modeling the position of comets with respect to the HCS, we conclude that an HCS boundary crossing possibly influenced three of these five events. For the two remaining events the comets were too distant from the HCS for a boundary crossing to have been the likely cause. At present, the SMEI data does not indicate any other discernable cause for these two tail disruptions.

[41] The observational evidence of comets and CMEs interacting is scant, so the full extent of these interactions is not well understood. Recent observations of comet pickup ions at large angular separations from the parent comets have been attributed to ion transport along ICME magnetic fields following the ICME passages over the comets [*Gloeckler et al.*, 2004]. Thus, detailed observations of ICME impacts on comets are needed to better define how comets interact with the ICME magnetic fields. As a space-based imager the SMEI observations can provide insight into these mechanisms. A follow-on paper [*Buffington et al.*, 2008] will provide more detailed analyses of the behavior of the comet tail motions as well as other disruption events. The analysis will include additional sources of data.

[42] **Note Added in Proof.** While this manuscript was under review, an article was published by *Vourlidas et al.* [2007] reporting on STEREO SECCHI observations of a CME interacting with Comet 2P/Encke on 20 April 2007 resulting in a plasma tail disconnection. The STEREO observations are the first such observations to appear in a refereed journal. However, the SMEI CME/comet observations discussed herein occurred in 2004 and had been previously presented and discussed at meetings [e.g., *Kuchar et al.*, 2006], although Vourlidas et al. do not make any reference to them.

## References

Altschuler, M. A., and G. Newkirk Jr. (1969), Magnetic fields and the structure of the solar corona, *Sol. Phys.*, 9, 131.

Arge, C. N., and V. J. Pizzo (2000), Improvement in the prediction of solar wind conditions using near-real time solar magnetic field updates, *J. Geophys. Res.*, 105, 10,465.

Arge, C. N., J. G. Luhmann, D. Odstrcil, C. J. Schrijver, and Y. Li (2004), Stream structure and coronal sources of the solar wind during the May 12th, 1997 CME, *J. Atmos. Sol. Terr. Phys.*, 66, 1295.

Biermann, L. (1951), Kometenschweife und solare korpuskularstrahlung, *Z. Ap.*, 29, 274.

Brandt, J. C., and R. D. Chapman (2004), *Introduction to Comets*, Cambridge Univ. Press, Cambridge, U. K.

Brandt, J. C., and M. Snow (2000), Heliospheric latitude variations of properties of cometary plasma tails: a test of the Ulysses comet watch paradigm, *Icarus*, 148, 52.

Brandt, J. C., F. M. Caputo, J. T. Hoeksema, M. B. Niedner Jr., Y. Yi, and M. Snow (1999), Disconnection events (DEs) in Halley's comet 1985–1986: The correlation with crossings of the heliospheric current sheet (HCS), *Icarus*, 137, 69.

Brueckner, G. E., et al. (1995), The large-angle spectroscopic coronagraph (LASCO), *Sol. Phys.*, 162, 357.

Buffington, A., D. L. Band, B. V. Jackson, P. P. Hick, and A. C. Smith (2006), A search for early optical emission at gamma-ray burst locations by the Solar Mass Ejection Imager (SMEI), *Astrophys. J.*, 637, 880.

Buffington, A., J. S. Morrill, P. P. Hick, R. A. Howard, B. V. Jackson, and D. F. Webb (2007), Analysis of the comparative responses of SMEI and LASCO, *Proc. SPIE Int. Soc. Opt. Eng.*, 6689, 1.

Buffington, A., M. M. Bisi, J. M. Clover, P. P. Hick, B. V. Jackson, and T. A. Kuchar (2008), Analysis of plasma-tail motions for comets c/2001 Q4 (NEAT) and c/2002 T7 (LINEAR) using observations from SMEI, *Astrophys. J.*, in press.

Calabretta, M. R., and E. W. Greisen (2000), Representations of celestial coordinates in FITS, *Astron. Astrophys.*, 395, 1077.

Eyles, C. J., G. M. Simnett, M. P. Cooke, B. V. Jackson, A. Buffington, P. P. Hick, N. R. Waltham, J. M. King, P. A. Anderson, and P. E. Holladay (2003), The Solar Mass Ejection Imager (SMEI), *Sol. Phys.*, 217, 319.

Gloeckler, G., F. H. A. Allegrini, D. J. Elliott, N. A. McComas, J. Schwadron, R. Geiss, R. von Steiger, and G. H. Jones (2004), Cometary ions trapped in a coronal mass ejection, *Astrophys. J.*, 604, L121.

Jackson, B. V., et al. (2004), The Solar Mass Ejection Imager (SMEI) mission, *Sol. Phys.*, 225, 177.

Jones, G. H., and J. C. Brandt (2004), The interaction of comet 153P/Ikeya-Zhang with interplanetary coronal mass ejections: Identification of fast ICME signatures, *Geophys. Res. Lett.*, 31, L20805, doi:10.1029/2004GL021166.

Kuchar, T. A., A. Buffington, T. A. Howard, C. N. Arge, P. P. Hick, B. V. Jackson, and D. F. Webb (2006), The evolution of comets in the heliosphere as observed by SMEI, *Eos Trans. AGU*, 87(52), *Fall Meet. Suppl.*, Abstract SH32A-08.

McComas, D. J., S. J. Blame, P. Barker, W. C. Feldman, J. L. Phillips, P. Riley, and J. W. Griffe (1998), Solar Wind Electron, Proton, and Alpha Monitor (SWEPAM) for the advanced composition Explorer spacecraft, *Space Sci Rev.*, 86, 563.

Mizuno, D. R., et al. (2005), Very high altitude aurora observations with the Solar Mass Ejection Imager, *J. Geophys. Res.*, 110, A07230, doi:10.1029/2004JA010689.

Owens, M., and P. Cargill (2004), Non-radial solar wind flows induced by the motion of interplanetary coronal mass ejections, *Ann. Geophys.*, 22, 4397.

Schatten, K. H. (1971), Current sheet magnetic model for the solar corona, *Cosmic Electrodyn.*, 2, 232.

Schatten, K. H., J. M. Wilcox, and N. F. Ness (1969), A model of interplanetary and coronal magnetic fields, *Sol. Phys.*, 9, 442.

Smith, C. W., M. H. Acuna, L. F. Burlaga, J. L'Heureux, N. F. Ness, and J. Scheifele (1998), The ACE magnetic field experiment, *Space Sci. Rev.*, 86, 613.

Smith, E. J. (2001), The heliospheric current sheet, *J. Geophys. Res.*, 106, 15,819.

St. Cyr, O. C., et al. (2000), Properties of coronal mass ejections: SOHO LASCO observations from January 1996 to June 1998, *J. Geophys. Res.*, 105, 18,169.

Tappin, S. J., et al. (2004), Tracking a major interplanetary disturbance with SMEI, *Geophys. Res. Lett.*, 31, L02802, doi:10.1029/2003GL018766.

Vourlidas, A., and R. A. Howard (2006), The proper treatment of coronal mass ejection brightness: A new methodology and implications for observations, *Astrophys. J.*, 642, 1216.

Vourlidas, A., C. J. Davis, C. J. Eyles, S. R. Crothers, R. A. Harrison, R. A. Howard, J. D. Moses, and D. G. Socker (2007), First direct observation of the interaction between a comet and a coronal mass ejection leading to a complete plasma tail disconnection, *Astrophys. J. Lett.*, *688*, 79.

Webb, D. F., et al. (2006), Solar Mass Ejection Imager (SMEI) observations of coronal mass ejections (CMEs) in the heliosphere, *J. Geophys. Res.*, *111*, A12101, doi:10.1029/2006JA011655.

Wegmann, R. (2000), The effect of some solar wind disturbances on the plasma tail of a comet: models and observations, *Astron. Astrophys.*, *358*, 759.

Yashiro, S., N. Gopalswamy, G. Michalek, O. C. St. Cyr, S. P. Plunkett, N. B. Rich, and R. A. Howard (2004), A catalog of white light coronal mass ejections observed by the SOHO spacecraft, *J. Geophys. Res.*, *109*, A07105, doi:10.1029/2003JA010282.

Yi, Y., R. J. Walker, T. Ogino, and J. C. Brandt (1996), Global magnetohydrodynamic simulation of a comet crossing the heliospheric current sheet, *J. Geophys. Res.*, *101*, 27,585.

————————————

C. N. Arge and J. C. Johnston, Space Vehicles Directorate, Air Force Research Laboratory, 29 Randolph Road, Hanscom AFB, MA 01731, USA.

A. Buffington, B. V. Jackson, and P. P. Hick, Center for Astrophysics and Space Sciences, University of California, San Diego, 9500 Gillman Drive, La Jolla, CA 92093, USA.

T. A. Howard, Physics Department, Montana State University, P. O. Box 173840, Bozeman, MT 59717, USA.

T. A. Kuchar, D. R. Mizuno, and D. F. Webb, Institute for Scientific Research, Boston College, 140 Commonwealth Avenue, Chestnut Hill, MA 02467, USA. (kuchar@bc.edu)

S. J. Tappin, National Solar Observatory/Sacramento Peak, P. O. Box 62, Sunspot, NM 88349, USA.